INFLUENCES OF TOOL TRAVEL SPEED ON TENSILE PROPERTIES OF UNDERWATER FRICTION STIR WELDED HIGH STRENGTH ARMOUR GRADE ALUMINIUM ALLOY JOINTS

* Sree Sabari S[1], Malarvizhi S[2] and Balasubramanian V[3]

[1]Research Scholar, Centre for Materials Joining and Research (CEMAJOR), Department of Manufacturing Engineering, Annamalai University, Annamalai Nagar – 608 002, Tamil Nadu, India. sreesabaridec2006@yahoo.co.in.
[2,3] Centre for Materials Joining and Research (CEMAJOR), Department of Manufacturing Engineering, Annamalai University, Annamalai Nagar – 608 002, Tamil Nadu, India.

ABSTRACT

AA2519-T87 armour grade aluminium alloy is relatively a new class of Al-Cu alloy which has high toughness, high strength to weight ratio and ballistic properties. Because of these properties, this alloy is recently used for fabricating light combat armour vehicles. However, fusion welding of this alloy will end up with solidification defects like porosity, hot cracking, etc. To overcome these problems, friction stir welding (FSW) process can be used. Though in FSW, the joining of materials takes place below the melting temperature, the heat generated is enough to coarsen or dissolve the strengthening precipitates in the age hardenable Al alloys. To avoid the detrimental precipitation behaviour, under water friction stir welding (UWFSW) process can be employed. The effect of tool travel speed (TTS) on heat input and resultant mechanical properties will be entirely different in conventional FSW and UWFSW process. Hence this investigation is carried out to study the effect of TTS on the stir zone characteristics and the resultant tensile properties of the UWFSW joints. From this investigation, it is found that the joint made using TTS of 30 mm/min exhibited superior tensile properties and this may be attributed to the lower heat generation, higher grain boundary strengthening and narrowing of the lower hardness distribution region (LHDR).

Key words: *Underwater friction stir welding, tool travel speed, microstructure, tensile properties, microhardness*

1. Introduction

The use of armour grade aluminum alloys in the military applications is of great interest in recent years to design and welding engineers for ensuring fail-safe design of light combat military vehicles [1]. Aluminium alloy AA2519 is a new class of armour grade aluminium alloy which has superior tensile properties, fracture toughness properties and ballistic properties. Because of these enhanced properties, AA2519 Al alloy is applied in the fabrication of light combat military vehicles [2]. Fusion welding of this age hardenable aluminium alloy results in the solidification defects. In addition, the inherent oxide layer formation at the surface limits the application of fusion welding [3]. The aforementioned problems can be avoided by employing the solid state friction stir welding (FSW) process, which does not involve in melting [4-7]. However, the thermal cycles prevailing during FSW results in grain coarsening and precipitate coarsening in the thermo-mechanical affected zone (TMAZ) and heat affected zone (HAZ). These changes in precipitate size and distribution result in poor joint performance because, the hardness of the age hardenable alloys are mainly depends on the presence of the fine precipitates [8, 9]. In FSW joint, the TMAZ and HAZ exhibited poor hardness and so termed as lower hardness distribution region (LHDR).

To control the heat related problems, underwater friction stir welding (UWFSW) process is employed [10]. It is a variant of FSW process, in which the water is used for cooling. The high heat dissipation capacity of water rapidly transfers the heat from the work piece which makes relatively lower heat supply to the TMAZ and HAZ [11]. By this way the width of the TMAZ and HAZ can be greatly reduced.

Though the UWFSW process will yield joints with superior properties, the process parameters has to be selected in such a way to attain defect free, sound joints [12, 13]. Therefore it is necessary to understand the effect of process parameters in UWFSW process. Tool travel speed is an important process parameter in this process which decides the heat generation and subsequently joint properties [14, 15]. Though the previous studies on UWFSW demonstrated the enhancement in strength and hardness properties, the

Corresponding Author - E- mail: sreesabaridec2006@yahoo.co.in

relationship between the process parameters on the joint quality, microhardness and the tensile properties has not yet systematically investigated [16, 17]. Hence in this investigation, an effort has been made to understand the effect of tool travel speed (TTS) on the stir zone formation and the resultant tensile properties of the UWFSW of AA2519 T87 aluminium alloy.

Table 1. Chemical composition (wt %) of AA 2519 T87 aluminium alloy

Cu	Mg	Mn	Fe	V	Si	Ti	Al
5.71	0.47	0.27	0.1	0.05	0.04	0.02	93

Table 2. UWFSW parameters and tool dimensions used in this investigation

Process Parameters	Values
Tool rotational speed (rpm)	1300
Tool travel speed (mm/min)	20, 25, 30, 35, 40
Pin length (mm)	5.7
Tool shoulder diameter (mm)	18
Pin diameter (mm)	5-6
Tool tilt angle, degree	2°
Pin Profile	Taper threaded cylindrical

2. Experimental Details

In this investigation, AA 2519-T87 aluminium alloy of 6 mm thick rolled plate was used as the parent metal. The chemical composition of the parent metal is listed in the Table 1. Joint configuration of 300 mm x 300 mm x 6 mm was used in this investigation. The plates were rigidly clamped and the water was filled in the tank so that the workpiece and the tool get immersed. UWFSW was carried out along the direction perpendicular to the rolling direction. The process parameters and welding conditions used to fabricate the joints are listed in table 2. In this phase of experimentation, the tool travel speed alone varied from 20 mm/min to 40 mm/min in steps of 5 mm/min keeping all other parameter constant.

After welding, the specimens required for characterization and testing were machined from the weld joint using the electrical discharge machine.

Microstructural examination was carried out using an optical microscope (OM) (Make: Metal Vision, India). The standard metallographic procedures were followed to prepare the specimens for microstructural analysis. The specimens were etched with standard Keller's reagent as per the ASTM E407 guidelines. The precipitation behaviour of the LHDR was studied using transmission electron microscope (TEM). A thin slice of specimens were extracted along the cross section using electro discharge machining process. The TEM specimens were polished to a thickness of 100 μm. The specimen of 3 mm diameter was extracted from the LHDR using a punching machine. The specimens were further polished to 10 μm using ion milling process to reveal the microstructure. The tensile specimens were cut perpendicular to the welding direction from the joint. The specimen preparation and the testing procedures were done as per the ASTM E8M-04 guidelines. Tensile testing was carried out using servo hydraulic controlled universal testing machine (Make: FIE-Blue Star, India; Model: UNITEK-94100). The transverse tensile properties such as yield strength, tensile strength and elongation of the UWFSW joints were evaluated. The tensile fracture surfaces were characterized using the scanning electron microscopy (SEM) (JEOL make, India). In order to observe the complete mapping of fracture path, the failed samples were extracted, polished and etched at the cross-section. OM is employed to reveal the full tensile fracture path. The Vickers microhardness tester (SHIMADZU, Japan; model HMV-2T) was used to measure the hardness at the mid thickness of the weld cross-section. The indenting load of 0.5 N was used for the dwell time of 15 s for recording the microhardness at various locations.
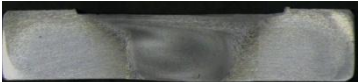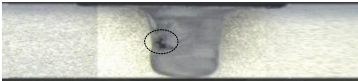
3. Results and Discussion

3.1 Macrostructures

The joint quality is further examined from the cross sectional micrographs (Table 3). The joints fabricated using the lower TTS of 20 mm/min, 25 mm/min and 30 mm/min show defect free stir zones where as the joints fabricated using higher TTS of 35 mm/min and 40 mm/min result in the defect formation in the stir zone. The defective samples are not fit for the service and so the defect free joints fabricated using TTS of 20 mm/min, 25 mm/min and 30 mm/min are alone considered for the further testing and characterization.

The joint quality of the UWFSW joint is mainly relying on the heat generation and the resultant material flow behaviour [18]. The extent of heat generation are categorized into three states namely, insufficient heat state, balanced heat state and excess heat state. With respect to the heat states, three material flow states namely, insufficient material flow state, balanced material flow state and excess material flow state will occur in the SZ. Therefore, by regulating the heat generation, the thermal softening and plasticization of material required for balance material flow can be attained. TTS is found to be a predominant parameter in FSW process which greatly influences the heat generation and material flow [19]. In this investigation, the defect free joints were obtained while using TTS

ranges from 20 mm/min to 30 mm/min. However, the defects are formed in the SZ at the higher TTS of 35 mm/min and 40 mm/min. The defect formation at the higher TTS is attributed to the attainment of insufficient heat generation and improper material flow state in the stir zone.

Table 3. Effect of tool travel speed on cross sectional macrographs

Tool travel speed, mm/min	Macrograph	Observation
20		Defect free stir zone
25		Defect free stir zone
30		Defect free stir zone
35		Tunnel defect at the AS
40		Tunnel defect at the AS

At lower TTS, long stirring time is available and so adequate heat is generated. The availability of the tool to generate heat and transport material is higher at the lower TTS. Therefore balance state of heat and material flow is achieved in the lower range of welding speeds. Increasing the TTS from 30 mm/min to 40 mm/min, would change the heat state from balanced to insufficient state. Due to less stirring time, limited tool rubbing and limited thermal softening takes place. Therefore the defect formation at the higher TTS is attributed to the attainment of insufficient heat and material flow states in the SZ.

During the plunging stage of UWFSW process, a dwell period is maintained to create a preheat zone at the leading edge of the tool. The preheat zone contributes two functions, first the preheat zone aid the tool to move freely without tool breakage and secondly, the material in the preheat zone extrude to rear end of the tool on tool forward to aid the defect free SZ formation. In general, due to the high heat dissipation capacity of water, the thermal softening is limited and so narrowed preheat zone is formed in the UWFSW process. In such circumstances, insufficient heat generation at higher TTS further narrowed the preheat zone. This is an additional reason for the defect formation in the joints fabricated using higher TTS.
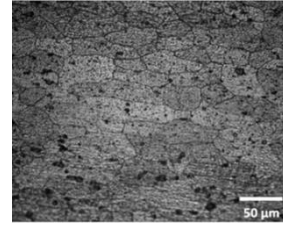

Fig. 1 Optical micrograph of parent metal

3.2 Microstructure

The micrograph of AA2519 Al alloy is characterized by the presence of coarse elongated grains oriented towards the rolling direction and exhibited average grain size of 49 μm (Figure 1 and Table 4). The optical micrographs of the three defect free joints are shown in Figure 2. The stir zone micrographs are characterized by the presence of fine grains, which are equi-axially oriented. The recrystallized grains are observed in all the three defect free joints (Figure 2a, 2b and 2c). Among the three stir zones, the joint fabricated using TTS of 20 mm/min shows larger grain diameter of 5.4 μm.

The AS-TMAZ (advancing side-thermo mechanically affected zone) and RS-TMAZ (retreating side-thermo mechanically affected zone) micrographs are characterized by severely deformed and upward oriented grains. The grains are pulled towards the SZ. The joint fabricated using TTS of 20 mm/min exhibit higher grain diameter of 56 μm and 57 μm in the AS-TMAZ and RS-TMAZ respectively. The joint fabricated using TTS of 25 mm/min shows the lower grain diameter of 50 μm in both AS-TMAZ and RS-TMAZ. There is not much appreciable grain coarsening observed in the HAZ. The average grain diameter of HAZ is measured as 49 μm which is equal to the parent metal grain size.

The stir zone is characterized by the presence of recrystallized grains. The tool stirring results in severe deformation and high thermal exposure in the SZ which promotes the recrystallization process [20, 21]. Therefore fine and equiaxed recrystallized grains were formed in the SZ. Because of the insufficient deformation and thermal exposure, recrystallization of grain cannot be occurred in the TMAZ. The microstructure in the TMAZ is characterized by the presence of upward elongated grains. The HAZ only experience the thermal exposure and no deformation takes place. So the grains exhibit a significant coarsening without any deformation. The microstructural features vary significantly with increase in TTS. As the TTS increases, the grain size in all region decreases. More specifically, the SZ and TMAZ have undergone significant decrement in the grain

diameter. On water cooling, the HAZ is narrowed and the heat input in the HAZ is very minimal to affect the microstructure so the grain size decrement on TTR increment is not significant. On the other hand, the heat input in the SZ and TMAZ is high enough to affect the microstructures irrespective of the water cooling because it exposed to direct contact with the tool rubbing. Due to long tool rubbing time, the joint fabricated using lower welding speed experience high heat input and so the grain size are higher in the respective regions.
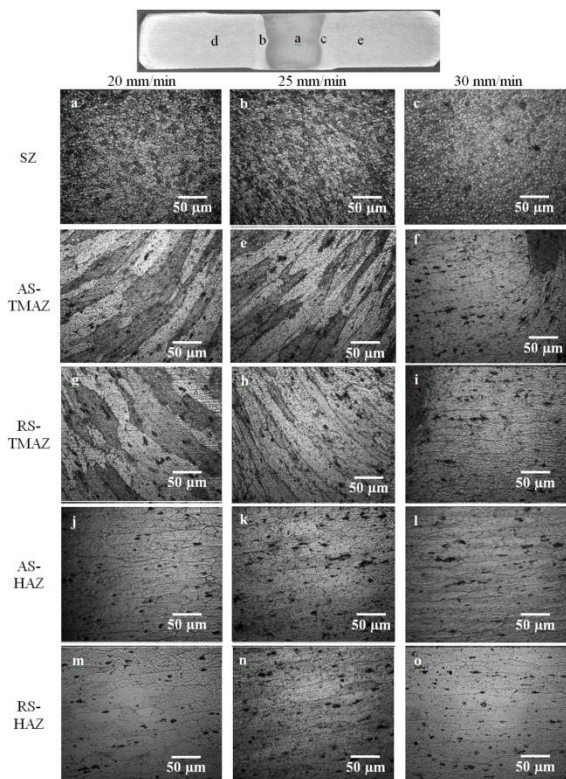

Fig. 2 Optical micrographs of various regions of UWFSW joints

Table 4. Average grain diameter distribution across the weld joint cross section

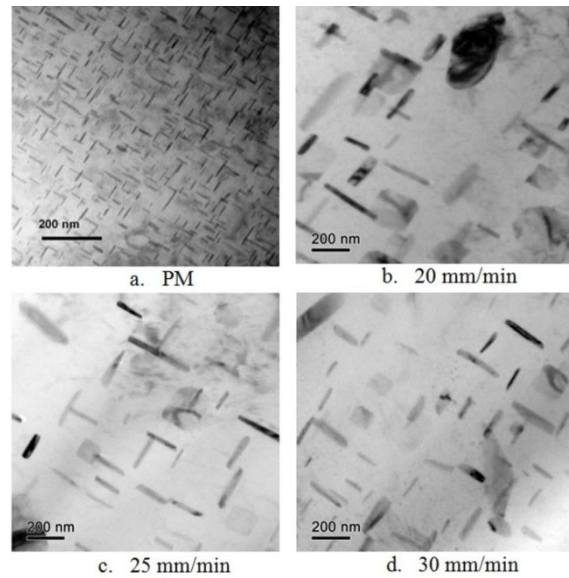| Tool travel speed, mm/min	SZ (µm)	AS-TMAZ (µm)	RS-TMAZ (µm)	AS-HAZ (µm)	RS-HAZ (µm)	PM (µm)
20	5.4	56	57	50	50	
25	4.2	55	55	49	49	49
30	3.3	50	50	49	49	

Fig. 3 TEM analysis in the PM and RS-TMAZ (LHDR)

Figure 3 shows the TEM images of the parent metal and RS-TMAZ. The parent metal composed of fine needle like precipitates which are normally oriented to each other. The precipitates are dense and evenly distributed over the aluminium matrix (Figure 3a). Figure 3b, 3c and 3d shows the precipitate distribution in the RS-TMAZ of joints fabricated using TTS of 20 mm/min, 25 mm/min and 30 mm/min. The volume fraction of the precipitates in the TMAZ regions is very lower than the parent metal. Moreover the size of the precipitates is coarser than the parent metal. It composed of precipitate free zone which resembles that the precipitates under gone dissolution. It is also important to notice that, increase in TTS increase the volume fraction and decrease the size of the precipitates. The high heat input and intense deformation at low TTS accelerate the aging process and thus exhibit large extent of dissolution or coarsening of precipitates.

3.3 Microhardness

The effect of TTS on microhardness profiles of UWFSW joints is shown in Figure 4. The "W" shaped hardness profiles are recorded at different TTS. The lower hardness is observed in the TMAZ on both the AS and RS of all the joints. The joint fabricated using TTS of 20 mm/min shows the lowest hardness of 86 HV whereas the joints fabricated using TTS of 25 mm/min and 30 mm/min recorded 88 HV and 98 HV respectively in the LHDR. It can be observed that, at constant tool rotational speed, increasing the TTS from

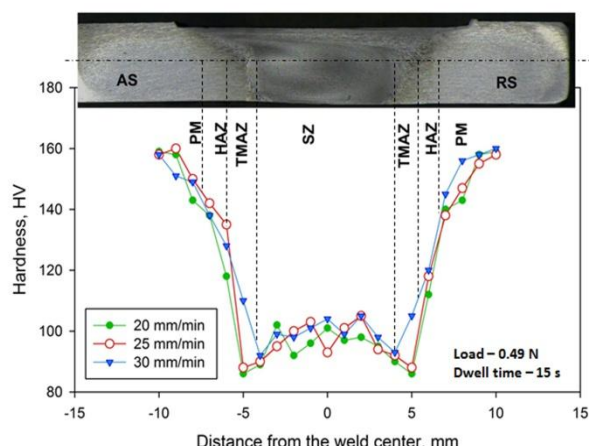20 mm/min to 30 mm/min increases the hardness of LHDR.

Fig. 4 Microhardness plot

It can also be noticed that the width of the LHDR decreases with increase in the TTS. As the TTS increases from 20 mm/min to 30 mm/min, the position of the LHDR moved towards the weld center. The joint fabricated using TTS of 30 mm/min recorded marginally higher hardness values in all the regions than the other joints. The hardness of the stir zones is higher than that of the TMAZ. The hardness in the SZ does not show significant variation due to various levels of TTS. Adjacent to the TMAZ, the HAZ shows sharp increment in the hardness on both AS and RS of the joints.

The mechanical properties of the joints are dependent on the microstructural features of the various regions. The grain size and the precipitates are the main microstructural feature characterized in this investigation. The relationship between the strength and the grain size is known from the Hall-Petch relation. The relationship states that the strength or hardness is inversely proportionally to the average grain diameter [22]. The strength contribution from the grain boundary strengthening varies with region to region of the UWFSW joint. The TMAZ exhibit the higher grain diameter and so it yielded lower hardness. The presence of coarse precipitates and precipitate free zone in TMAZ offers low resistance to the dislocation movement. Therefore the precipitation hardening in the TMAZ is lower.TMAZ is lower. Hence, the TMAZ is identified as the LHDR among the various regions of the joint. The fine grains of SZ results in massive amount of grain boundaries. Grain boundaries are the high energy regions and it also act as the barrier for the dislocation motion.

Table 5. Transverse tensile properties of parent metal and UWFSW joints

	0.2 % Yield strength (MPa)	Tensile strength (MPa)	Elongation in 50 mm gauge length (%)	Joint efficiency (%)	Fracture location
Parent metal	427	452	11.2	-	RS-TMAZ
20 mm/min	260	294	9.8	65	RS-TMAZ
25 mm/min	263	322	9.4	71	RS-TMAZ
30 mm/min	322	345	9.17	76	RS-TMAZ

Because of this reason, the SZ exhibit higher hardness than the TMAZ region in all the three defect free joints. The joint fabricated using the lower TTS of 20 mm/min recorded comparatively lower hardness in all the regions than it counter parts. The decrement in the hardness is attributed to the higher heat input and resultant larger grain size, low volume fraction of precipitates and presence of coarse precipitates. With increase in TTS the hardness increases because of the low heat input.

3.4 Tensile properties

The tensile properties like yield strength, ultimate tensile strength are presented in the Table 5. The parent metal (PM) exhibits the higher tensile strength of 452 MPa whereas the UWFSW joints exhibits lower tensile strength than the PM. The tensile strength of the joints increases with increase in TTS from 20 mm/min to 30 mm/min. The joint fabricated using the lower TTS of 20 mm/min exhibited lower tensile strength of 294 MPa which is 34 % lower than PM. The joint fabricated using tool TTS of 25 mm/min and 30 mm/min yielded 322 MPa and 345 MPa respectively. The joint efficiency is calculated as 65 %, 71 % and 76 % for the joints fabricated using TTS of 20 mm/min, 25 mm/min and 30 mm/min respectively. The joints fabricated using TTS of 20 mm/min, 25 mm/min and 30 mm/min yielded elongation of 9.8 %, 9.4 % and 9.17 % respectively. Increase in TTS slightly decreases the ductility of the joints.

The tensile strength of the joints varies with varying TTS. The tensile strength and the joint efficiency of the joint fabricated at 30 mm/min are higher than the joint fabricated using lower TTS of 20 mm/min and 25 mm/min. Comparatively higher grain boundary strengthening, relatively high volume fraction of precipitates and narrowed LHDR contributes to the higher tensile strength of joint fabricated using TTS of 30 mm/min. On tensile loading the grain boundaries and precipitates offers resistance to dislocation motion and thereby limit the plastic deformation.

3.5 Fracture surface

The contribution of LHDR in deciding the tensile strength of the joint is more evident from the tensile fracture analysis. Table 6 reveals the tensile fracture location of the tensile tested specimen. The cross sectional macrograph of the fractured specimen reveals the entire fracture path. It can be inferred from the images that the fracture path is apparently hardness dependent. The fracture path exactly falls along the LHDR. It can be clearly seen that the fracture occurred in the retreating side of the TMAZ in all the joints.

Table 6 Effect of tool travel speed on fracture path

Tool travel speed	Fracture path	Observation
20 mm/min		Fractured along the RS-TMAZ
25 mm/min		Fractured along the RS-TMAZ
30 mm/min		Fractured along the RS-TMAZ

Fig. 5 reveals the macro and micro level characterization of the tensile fracture surfaces. In all the joints, at the macro level, two different types of fracture patterns are observed. Flat like fracture surface is observed at the pin influenced region (PIR) and uneven surface is observed at the shoulder influenced region (SIR). The SEM images show the fracture surface at higher magnification. The joint fabricated using TTS of 20 mm/min and 25 mm/min show both fine dimples and few flat featureless surfaces. The joint fabricated using TTS of 30 mm/min shows fine populated dimples oriented towards the loading direction. This suggests that the joints are failed in the ductile mode.

During loading, the tensile load will concentrate on the weakest region of the joint. This load concentration phenomenon is called strain localization. Irrespective of varying the TTS, the tensile fracture is occurred in the TMAZ in all the joints. The fracture location shows exact correlated with the LHDR of the microhardness plot (figure 4 and table 6). The hardness and tensile strength shows similar obvious trends on varying the TTS. Regarding the ductile properties of the joint, due to the strain localization, the LHDR region alone contributes to elongate during tensile loading. Hence, all the joints exhibit lower elongation values than the parent metal.

In summary, the TTS must be chosen in a proper range to produce balanced (optimum) state of heat generation and material flow to yield defect free UWFSW joints. The present investigation demonstrates that either higher level or lower level of TTS leads to defect formation and yields poor joint properties. The defect formation is owing to the inadequate tool stirring and the poor joint properties are owing to the high heat input.
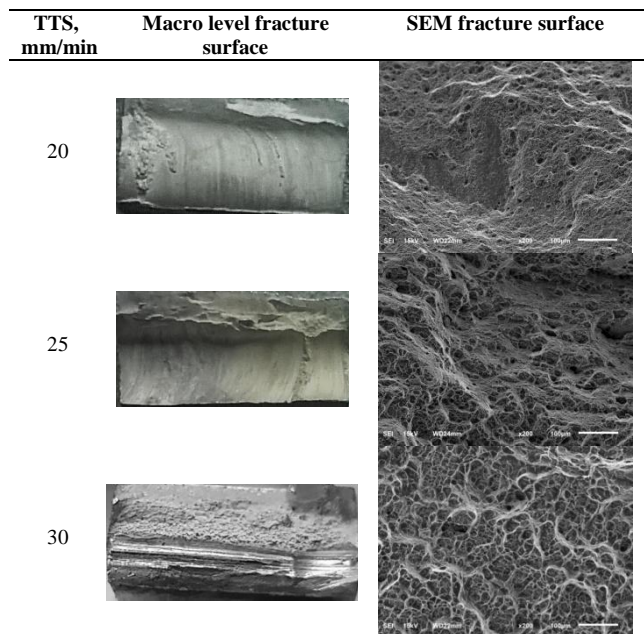
TTS, mm/min	Macro level fracture surface	SEM fracture surface
20		
25		
30		

Fig. 5 Fracture surface analysis

4. CONCLUSIONS

The effect of tool travel speed (TTS) on the stir zone characteristics and tensile properties of under water friction stir welded AA2519-T87 aluminium alloy joints was investigated and the following conclusions are derived:

1. Of the five joints fabricated, the joints fabricated within the TTS range of 20 to 30 mm/min yielded defect free stir zone formation. It is attributed to the attainment of balanced heat generation and proper material flow state during these welding conditions.

2. The joint fabricated using TTS of 30 mm/min exhibited tensile strength of 342 MPa and joint efficiency of 76 %, which is 7 % and 15 % higher than the joint fabricated using TTS of 20 mm/min and 25 mm/min respectively.

3. The presence of relatively finer grains in the stir zone, marginally higher hardness of stir zone and appreciably lower width of lower hardness region are the main reasons for the superior performance of the joint fabricated using TTS of 30 mm/min than other two joints.

ACKNOWLEDGEMENT

REFERENCES

1. *Babu N Karunakaran N and Balasubramanian V (2014), "Comparative evaluation of temperature distribution in GTAW and FSW joints of AA 5059 aluminium alloy", Journal of Manufacturing Engineering, Vol. 9(2), 71-76.*

2. *Fisher J James J Lawrence S K and Joseph R P (2002), "Aluminum alloy 2519 in military vehicles", Advanced Materials Process, Vol. 160, 43-46.*

3. *Sivaraj P Kanagarajan D and Balasubramanian V (2014), "Effect of post weld heat treatment on fracture toughness properties of friction stir welded AA7075-T651 aluminium alloy joints", Journal of Manufacturing Engineering, Vol. 9(2), 110-115.*

4. *Lakshmana Rao M Shyam P Kodali Suresh Babu P Rammohan T and Seenaiah Y (2014), "Experimental investigations on friction stir welding of Al2219", Journal of Manufacturing Engineering, Vol. 9(1), 45-48.*

5. *Venkatesan S Rajamani G P Balasubramanian V and Rajakumar S (2015), "S-N behaviour of friction stir welded AZ31B magnesium alloy joints", Journal of Manufacturing Engineering, Vol. 10, 10-16.*

6. *Arun Prasath and Razal Rose A (2015), "Investigation of mechanical and metallurgical properties of friction stir welded magnesium alloy", Journal of Manufacturing Engineering, Vol. 10, 81-85.*

7. *Manickam S and Balasubramanian V (2015), "Developing empirical relationships to predict the strength of friction stir spot welded AA6061-T6 aluminum alloy and copper alloy dissimilar joints", Journal of Manufacturing Engineering, Vol. 10, 207-214.*

8. *Christian Fuller B Murray Mahoney W Mike Calabrese and Leanna Micona (2010), "Evolution of microstructure and mechanical properties in naturally aged 7050 and 7075 Al friction stir welds", Materials Science and Engineering A, Vol. 527(9), 2233-2240.*

9. *Rui-dong Fu Zeng Qiang-sun Rui Cheng-sun Ying Li Hui-Jie Liu and Lei-liu (2011), "Improvement of weld temperature distribution and mechanical properties of 7050 aluminum alloy butt joints by submerged friction stir welding", Materials and Design, Vol. 32, 4825-4831.*

10. *Wang Kuai-she Wu Jia-lei Wang Wen Zhou Long-hai Lin Zhao-xia and Kong Liang (2012), "Underwater friction stir welding of ultrafine grained 2017 aluminum alloy", Journal of Central South University, Vol. 19, 2081-2085.*

11. *Hui-jie Zhang Hui-jie Liu and Lei Yu (2013), "Thermal modeling of underwater friction stir welding of high strength aluminum alloy", Transactions of Nonferrous Metals Society of China, Vol. 23, 1114-1122.*

12. *Zhang H J Liu H J and Yu L (2012), "Effect of water cooling on the performances of friction stir welding heat-affected zone", Journal of Material Engineering and Performance, Vol. 21, 1182-1187.*

13. *Liu Hui-jie Zhang Hui-jie Huang Yong-xian and Yu Lei (2010), "Mechanical properties of underwater friction stir welded 2219 aluminium alloy", Transaction of Nonferrous Metals Society of China, Vol. 20,1387-1391.*

14. *Liu H J Zhang H J and Yu L (2011), "Effect of welding speed on microstructures and mechanical properties of underwater friction stir welded 2219 aluminum alloy", Materials and Design, Vol. 32, 1548-1553.*

15. *Zhang Z Xiao B L and Ma Z Y (2014), "Influence of water cooling on microstructure and mechanical properties of friction stir welded 2014 Al-T6 joints", Materials Science and Engineering A, Vol. 614, 6-15.*

16. *Huijie Zhang and Huijie Liu (2013), "Mathematical model and optimization for underwater friction stir welding of a heat-treatable aluminum alloy", Materials and Design, Vol. 45, 206-211.*

17. *Hosseini M and Danesh Manesh H (2010), "Immersed friction stir welding of ultrafine grained accumulative roll-bonded Al alloy", Materials and Design, Vol. 31, 4786-4791.*

18. *Zhang Z Xiao B L Wang D and Ma Z Y (2011), "Effect of alclad layer on material flow and defect formation in friction-stir-welded 2024 aluminum alloy", Metallurgical and Materials Transactions A, Vol. 42(6), 1717-1726.*

19. *Saeid T Abdollah-Zadeh A Assadi H and Malek Ghaini F (2008), "Effect of friction stir welding speed on the microstructure and mechanical properties of a duplex stainless steel" Materials Science and Engineering A, Vol. 496(1), 262-268.*

20. *Feng Xiuli Liu Huijie and John Lippold C (2013), "Microstructure characterization of the stir zone of submerged friction stir processed aluminum alloy 2219", Materials Characterization, Vol. 82, 97-102.*

21. *Zhang H J Liu H J and Yu L (2011), "Microstructure and mechanical properties as a function of rotation speed in underwater friction stir welded aluminum alloy joints", Materials and Design, Vol. 32, 4402-4407.*

22. *Genevois C Deschamps A Denquin A and Doisneau Cottignies B (2005), "Quantitative investigation of precipitation and mechanical behaviour for AA2024 friction stir welds", Acta Materialia, Vol. 53(8), 2447-2458.*